

M.B. ÖZYİĞİT^{1,2*}, F. HAYAT², Y. KILIÇ¹, O. GÜNDÜZ¹

EFFECT OF BORON IN COLD ROLLED DP STEELS; FUNDAMENTALS OF METALLURGY & GENERAL PROPERTY MAP

Dual-phase (DP) steels with their dual phase microstructures (hard martensite and soft ferrite) are used in many industrial applications, especially in the automotive industry, thanks to their desired mechanical properties and formability. These properties are directly related to their phase distribution in microstructure obtained as a result of the production conditions. The most important step of the production of cold rolled DP steels is the annealing process. In this study, the effect of boron alloying with line scale heat treatment cycle on the microstructure and mechanical properties of cold rolled DP steel was investigated. For this purpose, mechanical test, formability and weldability tests were carried out. The materials were characterized by optical microscopy (OM) and scanning electron microscopy (SEM/EBSD) studies. According to the results, alloying with boron delays the formation of ferrite and pearlite/bainite during the cooling process and increases the martensite formation rate. Boron alloyed cold rolled DP steel shows improved yield and tensile strength without significant loss of elongation. On the other hand, alloying with boron does not have a detrimental effect on the weld properties.

Keywords: Boron alloying; inter-critical annealing; DP steels; microstructure; mechanical testing

1. Introduction

Dual phase (DP) steels are low carbon low alloy steels containing martensite islands dispersed in the main ferritic matrix in their microstructure that presents high strength and ductility properties together [1]. DP steels are highly preferred in weight reduction efforts but with high mechanical strength in the automotive industry due to their good formability properties as well as high strength that can reach different values depending on the hard phase (martensite and bainite) ratio [2-7].

Cold rolled dual phase steels are subject to a continuous annealing process after cold rolling to obtain the aimed microstructure (ferrite and martensite) properties. In the continuous annealing process of dual phase steels, the steel strip is heated up to a temperature within inter-critical temperature range and soaked at that temperature to ensure austenite nucleation and growth. The microstructure of the steel strip consists of ferrite and austenite phases at this stage. The strip is then slowly cooled down to the quenching temperature and then quenched. The quenching step is necessary for austenite transformation to martensite. The process is finalized by aging and air cooling [8-10].

LM and SEM methods are based on discrimination of the phases by the means of shape, colour and structure itself. Although they are extensive and easily applicable tools, they strongly depend on the depth of etching; etching time and etchant concentration. For getting quantitative results, the other most demanded technique is TEM. It gives more quantitative results yet these results are coming from a very definite and local area since it deals with nanometer sized components. Overall assumption of a microstructure formation again, is not applicable with TEM. TEM analysis mostly applicable for observing shape and thickness of the components in high magnifications [11]. All these disadvantages and deficiencies for regarding techniques may be achieved with EBSD. EBSD is a tool for correlating crystallographic informations of materials with the microstructure itself with the aid of certain tools it uses. Comparing all other tools numbered above, EBSD became more powerful and demanded in recent years.

The performance of DP steels mainly depends on the chemical composition and microstructural parameters such as phase volume fraction and distribution. The required mechanical properties of DP steels can be achieved with a reasonable alloy composition design at low cost. Many researchers have studied

¹ EREGLI IRON AND STEEL WORKS CO., R&D CENTER OF ERDEMİR, ZONGULDAK/TURKEY

² KARABUK UNIVERSITY, METALLURGICAL AND MATERIAL SCIENCE ENGINEERING, KARABÜK/TURKEY

* Corresponding author: mbozyigit@erdemir.com.tr; bulut.ozyigit@gmail.com



the effect of chemical composition on the mechanical properties of DP steels, but less research has been made with boron [8,12-16] Boron is generally used as a micro-alloying element in a number of steels in where it increases hardenability [15-17]. The effect of boron on the hardenability is related to its migration into austenite grain boundaries and inhibit grain boundary nucleation of ferrite. Therefore, its action is to delay the formation of ferrite relative to the formation of transformation products at lower temperature. In the production of dual-phase steels, inhibition of ferrite formation is expected to increase martensite yield [18].

Recently, car manufacturers have shown interest in boron alloying steels for extremely high strength levels [19]. Besides mechanical properties, corrosion resistance of steels is a critical factor for long-term durability of steels. The corrosion resistance of DP steels and their corrosion mechanism under harsh environments has already been explored by many researchers; however, reported findings sometime contradict to one another [20-24]. Both positive and negative influences of martensite volume fractions on corrosion resistance of DP steels have been reported. Sarkar et al. reported a decrease in corrosion resistance of micro-alloyed DP steels with the increase in martensite content, whereas Jha et al. [22] and Nadlene et al. [23] reported improved corrosion resistance of DP steels. Zhang et al. [24] found improved corrosion resistance in DP steels as compared to ferritic-pearlitic weathering steels. The effect of boron micro-alloying on corrosion resistance of DP steel has been reported by S. Kumar and R. Desai [25] that boron precipitation at the grain boundary and reduction in grain boundary energy of DPB steel could be one of the reasons for improved corrosion

Uthaisangsuk et al. [26] stated that the stretch flangeability property is important along with the mechanical properties in determining the formability property and this was determined by the hole expansion test. Since hole expansion rate (HER) is affected by the internal structure, two different steels, DP600 and DP800, were used in the study. It was shown that DP800 steel has lower HER than DP600 steel. This result was attributed to the higher martensite phase ratio and hardness in DP800 steel as well as the differences in chemical composition between these two steels.

When annealing intercritically, as is the case in DP steel production, the materials do not reach equilibrium during soaking. This implies that the strip speed is an important process parameter. A slower strip speed will lead to greater austenite formation and a harder material in the final. On the other hand, slower strip speed will also increase the time in the gas-jet section, leading to the formation of larger amount of new ferrite and thus a softer material. Mn and C increase the austenite content and consequently the hardness of the materials. Higher levels of Si (0.4 wt%) are required to retard the formation of new ferrite during cooling in the gas-jet section, prior to quenching [27].

Boron is frequently used in press hardening, wear resistant and heat-treated steels, as it increases hardenability by enabling more austenite to transform into hard phase at lower cooling rates. Above the A3 temperature, boron atoms diffuse to austenite grain boundaries, reducing grain boundary surface energy. The decrease in the grain boundary surface energy impedes/retards ferrite phase formation at the grain boundaries, which is likely to nucleate during cooling. Therefore, the bainite nose shifts to the right in the CCT (continuous cooling transformation) diagram of boron alloyed steels, and hard phase transformation can be obtained even at relatively low cooling rates. This outcome is utilized in press-hardened hot stamping steels by addition of 25-50 ppm boron [28,29]. It was observed that an addition of 0.0020% (20 ppm) boron in 0.15 C DP steel, which is produced in a continuous galvanizing line, increased the yield and tensile strength by ~150 MPa and reduced the total elongation by ~5%. It was also observed that the ratio of hard phase (martensite + bainite) increased in the final product [30].

As mentioned before, welding properties are very important for automotive industry. DP steels are joined by several welding methods. Resistance spot welding (RSW) is the main joint method of assembly auto body due to its high efficiency in processing thin DP steel sheets. A wide variety of DP steel sheets up to 3 mm thickness can be handled by the RSW method. RSW for DP steels is the simplest, fastest, and most controllable. Automotive industry uses RSW at several thousand welding points in each automotive body structures [31-33].

In this study, the effect of boron on phase transformation, microstructure, mechanical properties and formability properties of DP steels were investigated with a line scale heat treatment cycle.

2. Materials and method

Chemical composition design (TABLE 1) and prediction of heat treatment behavior of the steels used in the study were performed by JMatPro and ThermoCalc (2023b) softwares. Two heats were realized in the specified chemical compositions with (22 ppm) and without boron. Slabs of 200 mm thickness were annealed at 1250°C for 2-3 hours and then hot rolled to 4.0 mm with 840°C finishing and 610°C coiling temperature. The hot rolled coils were reduced to 1.9 mm thickness by cold rolling process. The cold rolled coils with ferritic pearlitic microstructure were further processed in a continuous galvanizing line according to the thermal cycle given in Fig. 1.

Boron-free and boron-alloyed materials were produced with the process parameters in Fig. 1. Mechanical properties of the steels were determined by tensile tests with a Zwick

TABLE 1

Chemical analysis of the steel used in the study (%wt)

Composition	%C	%Mn	%P	%Si	%Cr	%Ti	B (%)	%Fe
Base Composition (BC)	0.065	1.55	0.02	0.25	0.65	—	—	Balanced
Boron Added Composition (BAC)	0.065	1.55	0.02	0.25	0.65	0.025	0.0022	Balanced

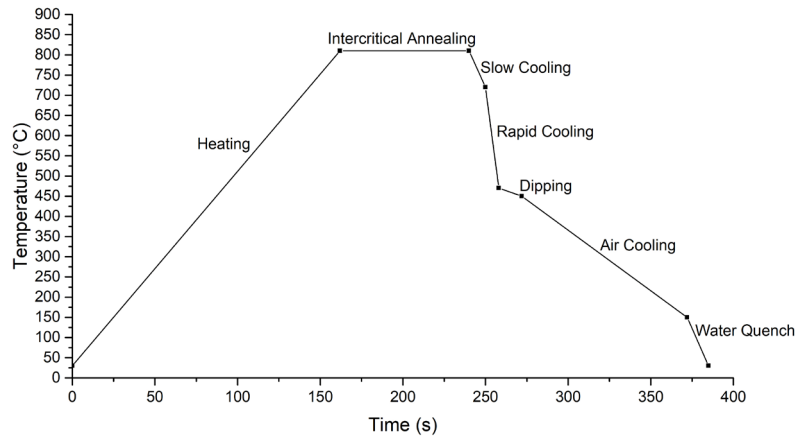


Fig. 1. Continuous galvanizing line heat treatment

250 kN tensile testing machine in accordance with the principles of ISO 6892-1 standard.

Microstructure characterizations were performed by using inverted type optical microscope (OM) (Nikon MA200) and the scanning electron microscope (SEM) (Jeol JSM 7100F). Samples for OM studies were prepared with grinding, polishing and etching by LePera solution. Ferrite and martensite phases can be detected in different colors by LePera solution etch, since it exhibits etching performance according to the carbon content of a phase.

In terms of discriminating phases of austenite and ferrite, it is the easiest job for EBSD to overcome. Since they have different crystallographic structure, body centered cubic (bcc) ferrite easily separated from face centered cubic (fcc) austenite. When it comes to differentiate same or similar crystallographies; martensite, ferrite and bainite it become a little bit tricky to achieve. In this circumstances, Kikuchi pattern quality information are referred. Kikuchi pattern quality is very sensitive and depended to lattice imperfections. The mean intensity of the Kikuchi patterns that formed with EBSD camera signal relative to the total intensity within the pattern can be used to distinguish the phases. So the strength of diffraction patterns which named as Image Quality (IQ) can be applied for discriminating phases. Every single measurement point in IQ maps corresponds to an individual pixel value that have spotted by EBSD camera. IQ charts are basically obtained from this mentioned measurements with the grayscale ranging from 1 to 255. The specimens for EBSD measurement were prepared with a basic metallographic preparation methods; cutting, embedding to hot pressed bakelite and finally mechanical polishing. Compact automated device Qpol 250 BOT was used for fully automated grinding and polishing steps including ultrasonic cleaning station. Final step of preparation was 15 minutes of colloidal-silica polishing with the diamond size of 0.04μ to get rid of the surface-relief which have been formed while mechanical polishing steps. After preparation steps, EBSD measurements were carried out for both samples on the cross-sections of ND-RD plane with a 70° pre-tilted specimen holder. EBSD mapping was performed with the field emission scanning electron microscope, JEOL JSM 7100F, equipped with a HKL Nordlys EBSD detector. The results were analyzed and

post-processed by EDAX/TSL OIM7 software. The accelerating voltage was 15 kV, working distance and beam intensity 17 mm and 14, respectively. The phase analysis procedure was adjusted with a camera resolution of 672×512 for $\times 1000$ microscope magnification that corresponds to $91 \times 121,5 \mu\text{m}$ selected area and camera was run at 2×2 binning mode with $0.18 \mu\text{m}$ step size.

Hole expansion test is widely used to determine the resistance of materials to form edge cracking. Test was carried out according to the ISO 16330 standard. The test is based on the principle of expanding the known initial hole diameter with a conical head using a maximum speed of 1 mm/sec and stopping when the first crack is fully formed along the section and measuring the final diameter. Final inside diameter of the hole is determined by at least two measurements in a perpendicular direction. Eq. (1) shows the hole expansion ratio calculation formula, D_f is final diameter, D_0 initial diameter of hole.

$$\begin{aligned} \text{Hole Expansion Ratio (\%, HER)} &= \\ &= [(D_f - D_0) / D_0] \times 100 \end{aligned} \quad (1)$$

The 3-point bending tests, which is another mechanical forming characterization method, were carried out according to the VDA238-100 standard with test apparatuses that can be integrated into the Zwick 250 kN tensile testing device. In this test, the aim is to determine the maximum bending angle that the material can reach with 3-point bending in the rolling direction of the material and perpendicular to the rolling direction. During bending test, when the minimum load drop of 30 N occurs after the maximum load is expressed as the position where the test is concluded. After this stage, if external bending angle measured on the material increases, (as the internal angle decreases), the performance of the material in the 3-point bending test increases.

The Nakajima test is a widely used and requested especially in the automotive industry. Nakajima, a.k.a. forming limit tests were carried out in accordance with the ISO 12004-2 standard within the scope of examining the forming properties of materials at different strain values. In this test, unlike the tensile test, the material is exposed to variable biaxial tension with different test geometries and molds. During the tests, just before the rupture is accepted as the limit and the major and minor strain values are obtained with the analysis work performed at this point.

The Nakajima test is a widely used and requested especially in the automotive industry.

3. Results and discussion

Phase distribution of the BC (Base Composition) and BAC (Boron Added Composition) DP steels during CGL process at 810°C and the amount of alloying elements that are in the austenite phase were determined by ThermoCalc software for thermodynamically initial investigation. Fe-C phase diagrams of the BC and BAC DP steels (TABLE 1) are given in Fig. 2.

In these diagrams dominant phase lines are introduced. It can be clearly seen both chemical compositions show the nearly same phase distribution. Phase ratio of the steels at 810°C and the amount of alloying elements dissolved by these phases were determined through the Fe-C phase diagrams (Fig. 3). The results show nearly same mass fraction of elements in stable phases.

The main difference between BC and BAC is stabilization of N. In BC, stabilization of N is done by Al and it is seen in inter-critical region (ALN) in Fig. 2. In BAC, stabilization has to be surely done by Ti which is a well-known best stabilization element for N since TiN (FCC_A1#2) forms during solidification at 1400°C. The main purpose of adding Ti element in the boron

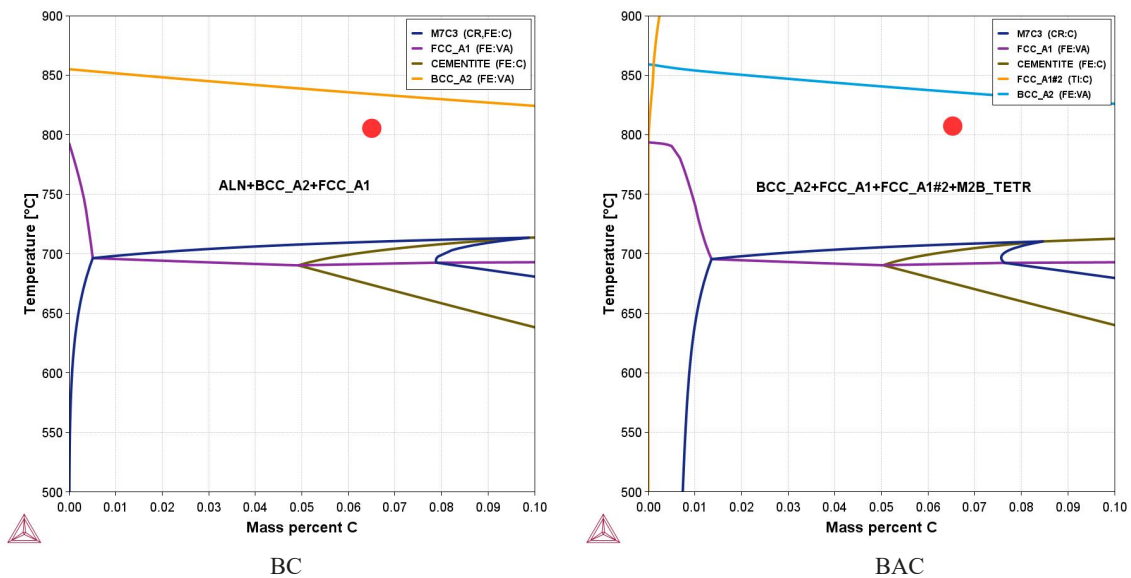


Fig. 2. BC and BAC Fe-C phase diagrams, which are drawn according to chemical compositions red points indicate annealing temperature

BC				BAC			
Stable Phases				Stable Phases			
BCC_A2#1	Moles	Mass	Volume Fraction	BCC_A2#1	Moles	Mass	Volume Fraction
Ferrite	0,74635	41,49892	0,41807	Ferrite	0,78824	43,82547	0,44132
Composition				Composition			
Component	Mole Fraction	Mass Fraction		Component	Mole Fraction	Mass Fraction	
Fe	0,97678	0,98107		Fe	0,97653	0,98088	
Mn	0,00963	0,00951		Mn	0,00979	0,00967	
Cr	0,00603	0,00564		Cr	0,00601	0,00562	
Si	0,00542	0,00274		Si	0,00539	0,00272	
Al	0,00137	0,00066		Al	0,00152	0,00074	
P	0,00061	0,00034		P	0,00059	0,00033	
C	0,00017	0,00004		C	0,00016	0,00003	
N	0,00000	0,00000		B	0,00001	0,00000	
				Ti	0,00000	0,00000	
				N	0,00000	0,00000	
Stable Phases				Stable Phases			
FCC_A1#1	Moles	Mass	Volume Fraction	FCC_A1#1	Moles	Mass	Volume Fraction
Ostenite	1,05524	58,49243	0,58173	Ostenite	1,01240	56,12023	0,55789
Composition				Composition			
Component	Mole Fraction	Mass Fraction		Component	Mole Fraction	Mass Fraction	
Fe	0,96210	0,96933		Fe	0,96185	0,96904	
Mn	0,01993	0,01975		Mn	0,02025	0,02007	
Cr	0,00758	0,00711		Cr	0,00755	0,00708	
Si	0,00460	0,00233		Si	0,00460	0,00233	
C	0,00501	0,00109		C	0,00492	0,00107	
Al	0,00059	0,00029		Al	0,00065	0,00032	
P	0,00018	0,00010		P	0,00018	0,00010	
N	0,00000	0,00000		B	0,00001	0,00000	
				Ti	0,00000	0,00000	
				N	0,00000	0,00000	

Fig. 3. Phase properties of BC and BAC at 810°C inter-critical region

analysis is to make maximum use of the hardenability feature of the boron element and to prevent BN precipitates to form during solidification and grain coarsening in hot rolling and annealing processes. Mechanical properties, phase distribution and particle size investigations show that boron can remain in solution without forming BN and contributes positively to the hardening property. In order to obtain the highest efficiency from boron added analysis [34] the amount of Ti in the chemical composition should be calculated according to Eq. (2) with the amount of N targeted. If Ti is not added, N is going to be stabilized with boron and precipitated with Al when boron is not added too, like BC.

$$Ti = 4.C + 3.42N + 1.5S \quad (2)$$

In addition, CCT diagrams were drawn at 810°C inter-critical annealing condition with JMatPro software (Fig. 4). CCT diagrams were drawn by JMatPro on the ratio of alloying elements dissolved in the austenite phase, which were roughly transformed during the heat treatment in the metastable region, that is the alloy amount per unit austenite.

Fig. 4 shows that ferrite and bainite lines have been largely displaced in BAC, so the amount of hard phase has increased in BAC. Boron diffuses to austenite grain boundaries and surrounds the area during inter-critical annealing. Thanks to these diffusion phenomena enrichment of carbon and formation of carbides

stops during cooling even slow rates. In addition to that ferrite formation diminished during cooling because surface energy of austenite grain boundary decreases. This led to the increase seen in tensile strength since martensite formation becomes easier during cooling. The results of these evaluations are given in the relevant headings.

3.1. Mechanical test results

Distributions of the mechanical properties of the samples are given in TABLE 2 and Fig. 5. It was determined that the yield and tensile strength values of the BAC is 4-6 kg/mm² higher than the BC analysis. The addition of 0.0020% (20 ppm) boron in 0.15 C DP steel increased the yield and tensile strength by ~15 kg/mm² and reduced the total elongation by ~5% [24]. In this study similar way of results were obtained. Main difference between is change of value in strength and total elongation. This because mainly alloying content such as C, Mn, Cr, etc. Because these elements are increases driving force of hard phase transformation and directly effects on hardenability.

Metallurgical explanation that is given above and micro-structure characterizations confirming this situation are also given in the next title. Another important issue of mechanical

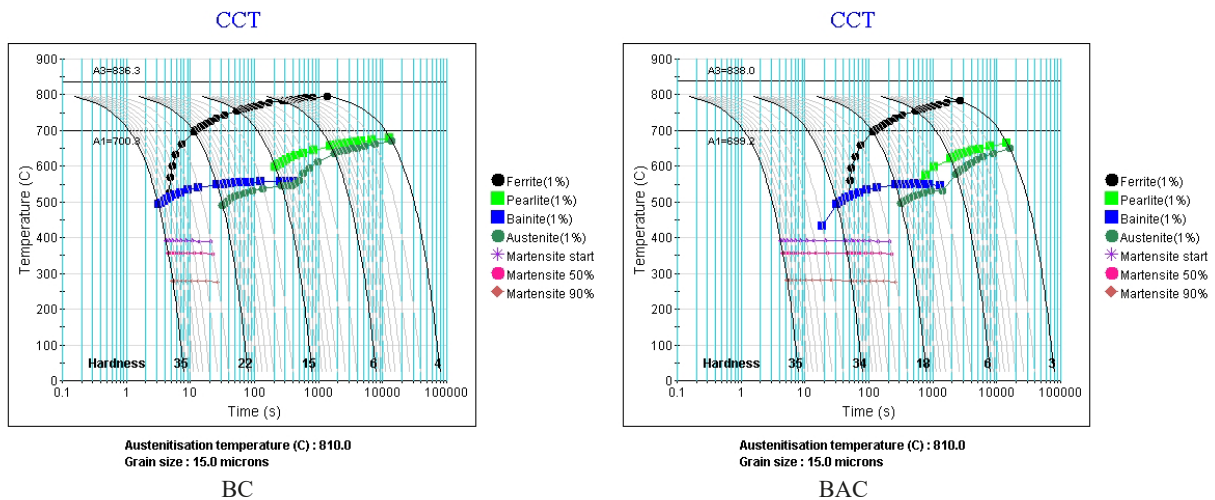


Fig. 4. CCT diagram depending on the amount of alloy that austenite will dissolve in case of annealing in the metastable region of BC and BAC. It can be clearly seen bainite nose shifts right side and martensite transformation can be occur with slower cooling rates in BAC

TABLE 2

Mechanical test results with quantitative numbers

Composition	Test No	Rolling Direction	m_E	$R_{p0.2}$ (Yield)	R_m (Tensile)	$n_{4-6/Ag}$	$r_{4-6/Ag}$	A_g (Uniform Elongation)	A_{80} (Total Elongation)
			GPa	MPa	MPa			%	%
BAC	1	Longitudinal	189	416.60	605.62	0.163	0.756	15.03	23.51
	2		192	418.77	606.17	0.161	0.769	14.73	23.30
	3		191	366.49	610.46	0.190	0.730	15.48	23.98
	4		191	364.87	612.75	0.191	0.703	15.47	24.15
BC	1	Longitudinal	189	357.25	542.40	0.185	0.771	16.95	27.74
	2		187	357.28	541.61	0.185	0.746	17.07	26.86
	3		187	344.29	537.14	0.198	0.839	18.01	27.18
	4		183	342.51	536.52	0.199	0.721	18.36	28.03

properties is the total elongation. Despite the increased strength in the BAC steel, the total elongation value is similar to the BC steel, which shows lower yield and tensile strength. These results indicate that high strength and elongation properties expected from DP steels can be achieved with low alloy contents and micro alloying with boron.

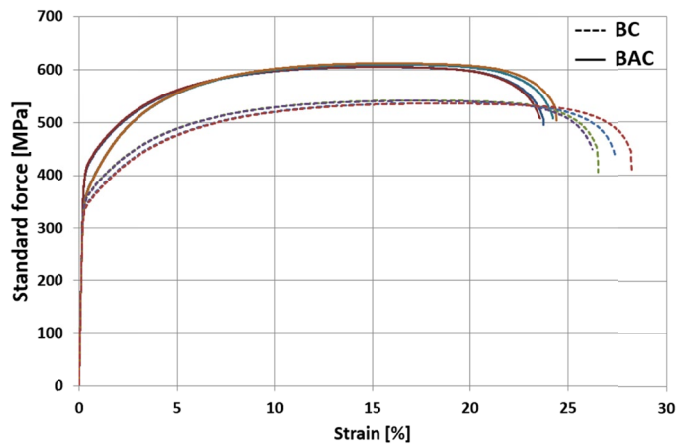


Fig. 5. Mechanical test results

3.2. Microstructure characterization

Microstructure images of samples taken from CGL mass productions were etched with LePera and martensite (white colored islets) ratio were determined. As expected, it was determined; microstructural investigations showed that the martensite ratio in BAC steel (14%) was higher than BC steel (9%), supporting the mechanical test results (Fig. 6). In addition, the ferrite grain size in BAC steel (6.8 μm) is finer than the BC steel (7.94 μm). Finer grain size the only mechanism that improves strength and toughness together.

SEM investigations carried out to determine the distribution of the secondary hard phase. SEM showed the existence of bainite phase in the BC DP steel (Fig. 7). This is not unexpected as CCT diagram of the BC DP steel showed that even at high

cooling rates bainite formation was possible (Fig. 4). It is thought that isothermal heat treatment (450–470°C/4–12 sec) occurring during the galvanizing stage in zinc pot, the CGL process promoted the formation of the bainite phase.

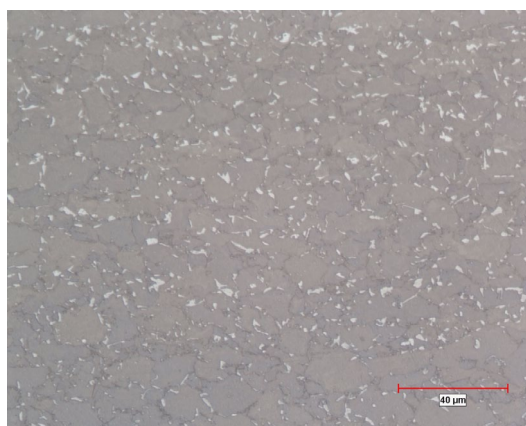
When evaluating phases with EBSD, one should notice that martensite has the lowest image quality and the amount of its lattice defects increases with the increase of its carbon content [35]. However dissociation of bainite from ferrite is the main challenge as they have similar lattice defects. Bainite has lower IQ than ferrite, as it contains a larger amount of imperfections in the crystal lattice. But there is no certain number of IQ value to refer this discrimination. To overcome this problem different mapping techniques can be used.

According to Zaefferer et al. (2010), common confusion arises because of having similar pixel values for different phases. For example, inside martensitic regions some pixels have maximum IQ value, whereas the ferritic region near the boundaries exhibits lower values. This results in considerable inaccuracy in discrimination [36]. To avoid this problem, in this paper grain average image quality (GIQ) is used. During averaging, pixels adjacent to boundaries are disregarded to minimize the influence of boundary or grain size. IQ and GIQ images and their corresponding profiles of samples are given in Fig. 8 and Fig. 9.

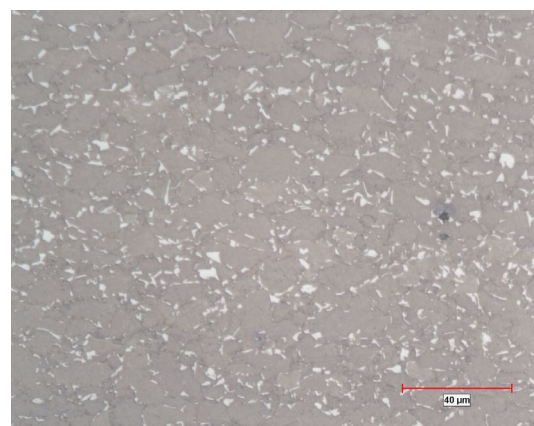
In Figs. 8a and 8c, IQ maps of the samples BC and BAC are presented. Figs. 8b and 8d are the IQ chart of the samples BC and BAC, respectively. In IQ charts change of the peak positions point out the phase transitions inside the same crystalline structure.

If the change in the peak position on the same chart is more than one, that is, if there is more than one peak point, it can be considered that there is a multi-phase transformation in the structure. In Fig. 8b, one can see that between ferrite and martensite transition there is an obvious another peak point at 130 that can be referred as bainitic transition for sample BC. It is of course not widespread over the histogram since the ratio of the bainitic transition is low. Fig. 8d, sample BAC does not show such kind of second transition peak point.

GIQ maps are used for ferrite and secondary phase (martensite and bainite) separation. From the GIQ charts a threshold



BC
9% Martensite; Grain Size: 7.94 μm



BAC
14% Martensite; Grain Size: 6.8 μm

Fig. 6. Microstructural investigations of BC and BAC GI steel

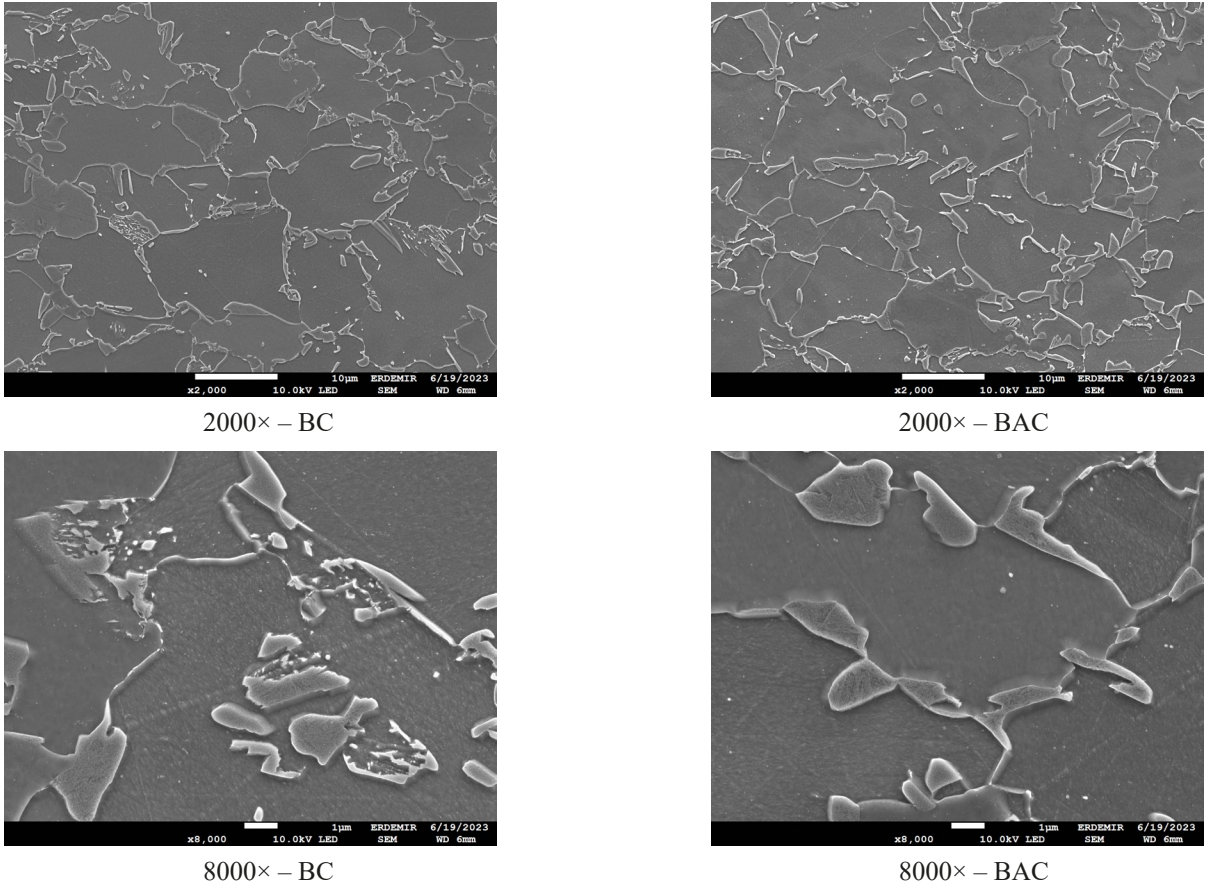


Fig. 7. SEM image of BC and BAC steel. (M: Martensite; F: Ferrite; B: Bainite)

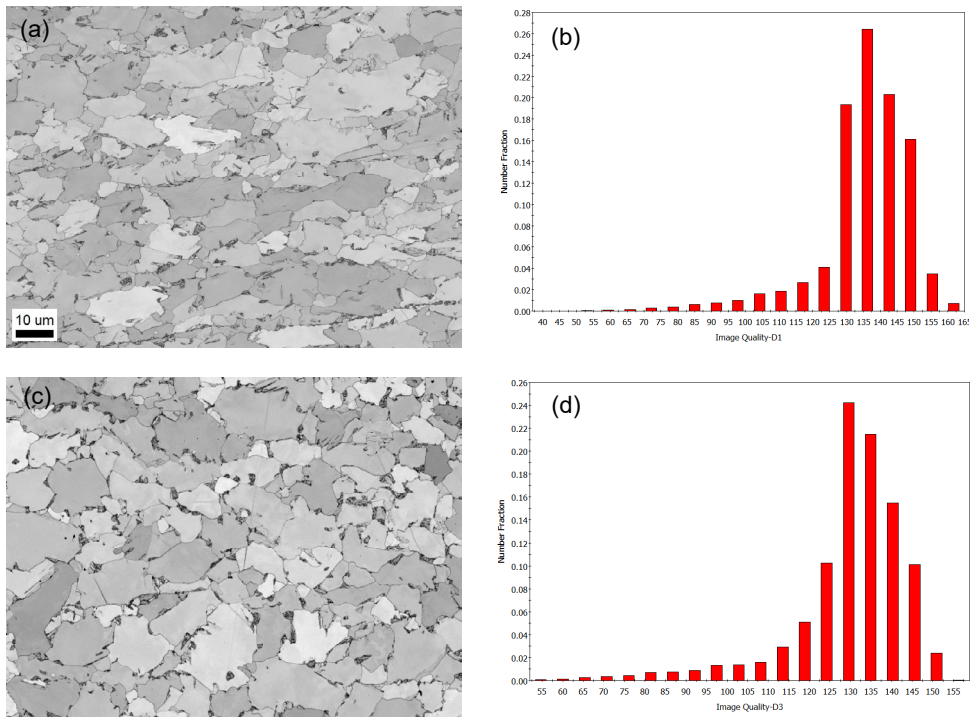


Fig. 8. IQ maps and their corresponding IQ charts for the sample BC (a,b) and BAC (c,d)

value is determined separately for both of the samples. When determining a threshold value as a ferrite separator it is important not to include any secondary phase inside that chosen threshold.

Trial and error method for assigning specific threshold could be useful for the circumstances. Fig. 9 shows the GIQ maps and their corresponding charts for the samples BC and BAC,

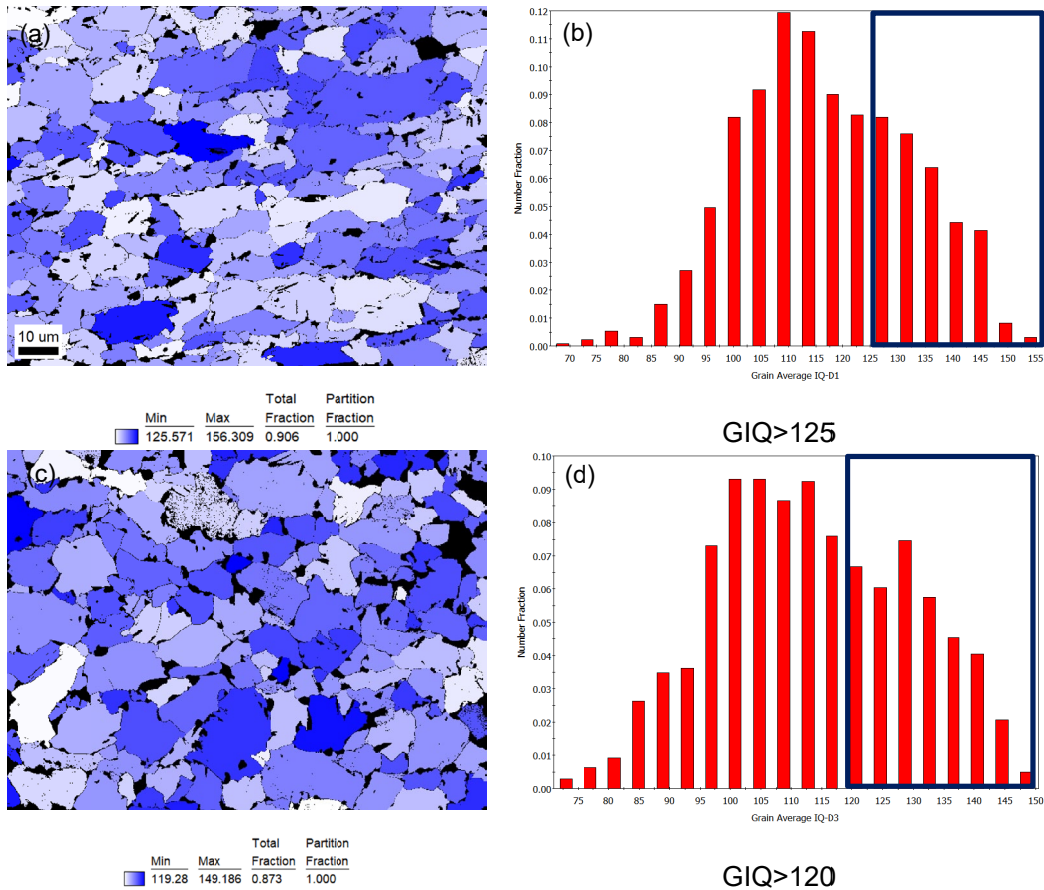


Fig. 9. GIQ maps and their corresponding GIQ charts for the sample BC (a,b) and BAC (c,d). Black rectangular boxes show the accepted threshold values for individual samples

respectively. Black rectangular boxes show the selected threshold values for corresponding GIQ maps. When the right threshold value is obtained, ferrite ratios for samples are shown in Fig. 9a as BC; Fig. 9c as BAC. Since grain averaging method is used, all pixels of the individual grain turn into same exact value and they are indicated a colour scale from white to blue as pattern quality increases from 1 to 255. Rest of the black spotted areas are secondary phases. For sample BC, ferrite fraction is acquired

as 90% while for sample BAC it is 87% which means total secondary phase fraction for BC is 10%, for sample BAC, 13%.

Since there is no significant bainite formation for sample BAC, bainite fraction is only measured for sample BC with GIQ method as shown in Fig. 10. The selected threshold value is between 90-125 and the bainite volume fraction is 2%.

The lower hard phase ratio, the bainite phase, which is softer than martensite, caused the strength of the BC DP steel to be relatively lower than the BAC DP steel. As seen characterization results, BAC DP steel has stable martensite phase formation. Also there is not any bainite formation. As mentioned before boron microalloying promotes martensite formation with diminishing ferrite and perlite/bainite formation. By this way mechanical properties are improved.

3.3. Formability properties

In the modelling of cold press behaviour of materials, besides mechanical tests, forming limit diagrams are used in order to determine the formability properties. Examining the forming properties of materials at different strain values is directly related to the press performance of the material. Forming limit diagrams of the BAC DP steel and a steel (EN 10338 Cold Rolled DP600) with similar mechanical properties are compared in Fig. 11. It is seen that strain distributions of both steels are close.

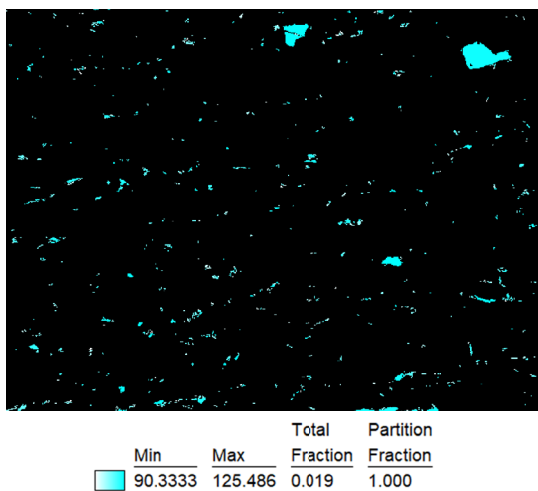


Fig. 10. GIQ map to obtain bainite fraction for sample BC with the selected threshold value 90-125

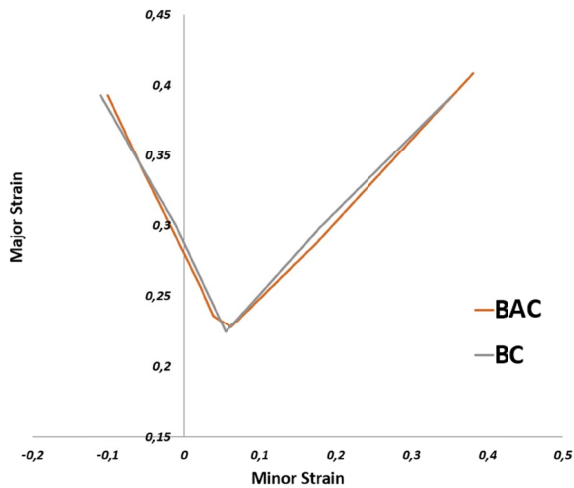


Fig. 11. Forming limit diagram

However, it was observed that the BAC DP steel exhibited negligibly worse results in the hole expansion and 3-point bending (TABLE 3) tests compared to the BC DP steel. The hole expansion test gives information about the stretch-flangeability resistance in materials and is directly related to the micro structure. The high amount of hard phase in the BAC DP steel caused a weakening in the edge tear resistance. Hole expansion ratio of BC and BAC are in average 63,3% and %42 respectively. Since the increase in the martensite phase also increases the yield strength, it was determined that there was a relatively worse shaping behavior in the boron analysis in the 3-point bending tests but both hole expansion ratio and 3-point bending angle of BAC, quite enough for DP600 grade that is used for automotive design works.

TABLE 3

3-point bending internal bending angle

Test Direction	Base Composition	Boron Added Composition
Longitudinal-1	44°	53°
Longitudinal-2	45°	55°
Longitudinal-3	45°	52°
Transverse-1	43°	45°
Transverse-2	42°	45°
Transverse-3	42°	42°

4. Conclusions

In this study, effect of boron addition to DP steel composition has been investigated. The boron addition helps to design lean chemical compositions reducing the content of other alloying elements (C, Mn, P, Cr, etc.) and could be used for weight and cost reduction works in automotive industry.

The key outputs proven by this study are as follows.

- Boron retards ferrite nucleation at the austenite grain boundaries during cooling stage of heat treatment in the intercritical region of dual-phase steels, which promotes hard phase transformation.

- Pearlite and bainite are found as secondary phases in the microstructure of BC. In BAC, however, most of the secondary hard phases belong to the martensite phase, due to the contribution of boron to the transformation of the martensite phase.
- At the same annealing temperature, in the intercritical region, the amount of austenite formation in BAC steel is lower than in BC, so the stability of the austenite phase is higher than in BAC, which affects the final product properties.
- As a result, boron microalloying is recommended for the production of dual-phase steels due to its positive contributions to mechanical strength and corrosion resistance.

Acknowledgments

The authors gratefully acknowledge the support of the Ereğli Iron & Steel Works Co and my colleagues Dilara Özyiğit and Mustafa Alp Yalçın.

REFERENCES

- [1] C.T. Sezgin, F. Hayat, The microstructure and mechanical behavior of trip 800 and dp 1000 steels welded by electron beam welding method. *Soldagem e Inspecao* **25**, 1-12 (2020). DOI: <https://doi.org/10.1590/0104-9224/SI25.26>
- [2] C.T. Sezgin, K. Üniversitesi, Investigation of Fracture Surface of Different Metals Welded by Resistance Spot Welding. [Online]. Available: <https://www.researchgate.net/publication/348817981>
- [3] F.D. Murari, A.L.V. Da Costa E Silva, R.R. De Avillez, Cold-rolled multiphase boron steels: Microstructure and mechanical properties. *Journal of Materials Research and Technology* **4**, 2, 191-196, Apr. (2015). DOI: <https://doi.org/10.1016/j.jmrt.2014.12.001>
- [4] M.C. Pantilimon et al., Preliminary Structures Assessment of Some TRIP Steels. *Archives of Metallurgy and Materials* **68**, 2, 491-498 (2023). DOI: <https://doi.org/10.24425/amm.2023.142427>
- [5] J. Park et al., Austenitic Stability And Strain-Induced Martensitic Transformation Behavior of Nanocrystalline FeNiCrMoC HSLA Steel. *Archives of Metallurgy and Materials* **68**, 1, 77-80 (2023). DOI: <https://doi.org/10.24425/amm.2023.141475>
- [6] S.H. Shin, S.G. Kim, B. Hwang, Application of artificial neural network to predict the tensile properties of dual-phase steels. *Archives of Metallurgy and Materials* **66**, 3, 719-723 (2021). DOI: <https://doi.org/10.24425/amm.2021.136368>
- [7] A. Skowronek, A. Kozłowska, A. Grajcar, M. Morawiec, Microstructure-properties relationship and mechanical stability of retained austenite in thermomechanically processed medium-C TRIP steel at different deformation temperatures. *Archives of Metallurgy and Materials* **65**, 2, 941-949 (2020). DOI: <https://doi.org/10.24425/amm.2020.132842>
- [8] M.D. Geib, D.K. Matlock, G. Krauss, The Effect of Intercritical Annealing Temperature on the Structure of Niobium Microalloyed Dual-Phase Steel.
- [9] G.R. Speich, V.A. Demarest, R.L. Miller, Formation of Austenite During Intercritical Annealing of Dual-Phase Steels.

- [10] M. Šebek, P. Horňák, P. Zimovčák, S. Longauer, Microstructure evolution and mechanical properties of C-Mn cold rolled dual phase steel after continuous annealing process in laboratory conditions. *Archives of Metallurgy and Materials* **59**, 2, 821-824 (2014). DOI: <https://doi.org/10.2478/amm-2014-0140>
- [11] M.S. Baek, K.S. Kim, T.W. Park, J. Ham, K.A. Lee, Quantitative phase analysis of martensite-bainite steel using EBSD and its microstructure, tensile and high-cycle fatigue behaviors. *Materials Science and Engineering: A* **785**, May (2020). DOI: <https://doi.org/10.1016/j.msea.2020.139375>
- [12] Q. Meng, J. Li, J. Wang, Z. Zhang, L. Zhang, Effect of water quenching process on microstructure and tensile properties of low alloy cold rolled dual-phase steel. *Mater. Des.* **30**, 7, 2379-2385, Aug. (2009). DOI: <https://doi.org/10.1016/j.matdes.2008.10.026>
- [13] S. Sun, M. Pugh, Properties of thermomechanically processed dual-phase steels containing fibrous martensite, (2002). [Online]. Available: www.elsevier.com/locate/msea
- [14] B. Demir, M. Erdoğan, The hardenability of austenite with different alloy content and dispersion in dual-phase steels. *J. Mater. Process Technol.* **208**, 1-3, 75-84, Nov. (2008). DOI: <https://doi.org/10.1016/j.jmatprotec.2007.12.094>
- [15] N. Shikana, M. Kurihard, H. Tagaw, Thermec-88, I. Tamura, ed., in *Iron and Steel Institute of Japan*, Tokyo, pp. 98-105 (1988).
- [16] M.K. Koul, C.L. McVicker, A new look at boron steels. *Metal Progress* **110**, 11, 2-8, (1976).
- [17] M. Packo et al., State of strain and development of microstructure of 22mnb5 steel and al-si coating during deep drawing of automotive b pillar. *Archives of Metallurgy and Materials* **66**, 2, 601-608 (2021). DOI: <https://doi.org/10.24425/amm.2021.135897>
- [18] X.P. Shen, R. Priestner, Effect of Boron on the Microstructure and Tensile Properties of Dual-Phase Steel.”
- [19] “Steel Offers Durable, Cost-Effective Solutions for Automotive Vehicles.” <https://www.steel.org/steel-markets/automotive/> (accessed Aug. 03, 2023).
- [20] R. Khondker, A. Mertens, J.R. McDermid, Effect of annealing atmosphere on the galvanizing behavior of a dual-phase steel. *Materials Science and Engineering: A* **463**, 1-2, 157-165, Aug. (2007). DOI: <https://doi.org/10.1016/j.msea.2006.09.116>
- [21] P.P. Sarkar, P. Kumar, M.K. Manna, P.C. Chakraborti, Microstructural influence on the electrochemical corrosion behaviour of dual-phase steels in 3.5% NaCl solution. *Mater. Let.* **59**, 19-20, 2488-2491, Aug. (2005). DOI: <https://doi.org/10.1016/j.matlet.2005.03.030>
- [22] B.K. Jha, R.A. Vats, S.V. Dwivedi, Structure-property correlation in low carbon low alloy high strength wire rods/wires containing retained austenite. *Transactions of the Indian Institute of Metals* **49**, 3, 133-142, Jun. (1996).
- [23] R. Nadlene, H. Esah, M.A. Norliana, M.A. Mohd Irwan, Study on the Effect of Volume Fraction of Dual Phase Steel to Corrosion Behaviour and Hardness. *International Scholarly and Scientific Research & Innovation* **5**, 2, 393-396 (2011).
- [24] C. Zhang, D. Cai, B. Liao, T. Zhao, Y. Fan, A study on the dual-phase treatment of weathering steel 09CuPCrNi. *Mater. Lett.* **58**, 9, 1524-1529, Mar. (2004). DOI: <https://doi.org/10.1016/j.matlet.2003.10.018>
- [25] S. Kumar, R. Desai, Effect of Boron Micro-alloying on Microstructure and Corrosion Behavior of Dual-Phase Steel. *J. Mater. Eng. Perform.* **28**, 10, 6228-6236, Oct. (2019). DOI: <https://doi.org/10.1007/s11665-019-04364-w>
- [26] V. Uthaisangsuk, U. Prahl, W. Bleck, Stretch-flangeability characterisation of multiphase steel using a microstructure based failure modelling. *Comput. Mater. Sci.* **45**, 3, 617-623, May (2009). DOI: <https://doi.org/10.1016/j.commatsci.2008.06.024>
- [27] D.K. Matlock, Correlation of Processing Variables with Deformation Behavior of Dual-Phase Steels. In *Structure and Properties of Dual-Phase Steels*, New York, (1979).
- [28] J. Bian, H. Mohrbacher, Novel Alloying Design for Press Hardening Steels With Better Crash Performance.
- [29] H. Hagenah, M. Merklein, M. Lechner, A. Schaub, S. Lutz, Determination of the mechanical properties of hot stamped parts from numerical simulations. In *Procedia CIRP*, Elsevier pp. 167-172, (2015). DOI: <https://doi.org/10.1016/j.procir.2015.06.031>
- [30] E. Bocharova, K. Khlopkov, R. Sebal, Effect of microalloying elements on phase transformation, microstructure and mechanical properties in dual-phase steels. In *Materials Science Forum*, Trans Tech Publications Ltd, p. 483-488 (2017). DOI: <https://doi.org/10.4028/www.scientific.net/MSF.879.483>
- [31] M. Shariati, M.J. Maghrebi, Experimental study of crack growth behavior and fatigue life of spot weld tensile-shear specimens. *Journal of Applied Sciences* **9**, 3, 438-448 (2009). DOI: <https://doi.org/10.3923/jas.2009.438.448>
- [32] F. Hayat, The effects of the welding current on heat input, nugget geometry, and the mechanical and fractural properties of resistance spot welding on Mg/Al dissimilar materials. *Mater. Des.* **32**, 4, 2476-2484, Apr. (2011). DOI: <https://doi.org/10.1016/j.matdes.2010.11.015>
- [33] M.K. Kulekci, Fracture toughness of friction stir welded joints of AlCu4SiMg aluminium alloy. (2005). [Online]. Available: <https://www.researchgate.net/publication/264051481>
- [34] B. Białobrzaska, R. Dziurka, Effect of Boron Accompanied by Chromium, Vanadium and Titanium on the Transformation Temperatures of Low-Alloy Cast Steels. *Archives of Metallurgy and Materials* **68**, 1, 257-267 (2023). DOI: <https://doi.org/10.24425/amm.2023.141502>
- [35] K. Zhu, D. Barbier, T. Lung, Characterization and quantification methods of complex BCC matrix microstructures in advanced high strength steels. *J. Mater. Sci.* **48**, 1, 413-423, Jan. (2013). DOI: <https://doi.org/10.1007/s10853-012-6756-9>
- [36] P. Romano, “EBSD as a tool to identify and quantify bainite and ferrite in low-alloyed Al-TRIP steels” (2008).